Journal of Alloys and Compounds 989 (2024) 174402

Contents lists available at ScienceDirect

Journal of Alloys and Compounds

journal homepage: www.elsevier.com/locate/jalcom

Ferrite doped sucrose-derived porous carbon composites inspired by Pharaoh's Serpent for broadband electromagnetic wave absorption

Heng Yang [a], Xin Jiang [b], Jiuxiao Sun [a], Bin Zhang [a,e,*], Xiaogang Su [c], Qilei Wu [d], Zhengyao Qu [e,**], Siqi Huo [f]

[a] Hubei Key Laboratory for New Textile Materials and Applications, School of Materials Science and Engineering, Wuhan Textile University, Wuhan 430200, China
[b] School of Materials Science and Engineering, Wuhan University of Technology, Wuhan 430070, China
[c] School of Materials Science and Engineering, North University of China, Taiyuan 030051, China
[d] Science and Technology on Electromagnetic Compatibility Laboratory, China Ship Development and Design Centre, Wuhan 430064, China
[e] State Key Laboratory of Silicate Materials for Architectures, Wuhan University of Technology, Wuhan 430070, China
[f] Center for Future Materials, School of Engineering, University of Southern Queensland, Springfield 4300, Australia

ARTICLE INFO

Keywords:
Porous structure
Lightweight
Biomass carbon sources
Carbon catalytic reduction
Broadband microwave absorption

ABSTRACT

This paper presents a straightforward and intriguing approach for designing wide bandwidth, lightweight, and tunable electromagnetic wave (EMW) absorbing materials. Drawing inspiration from the "Pharaoh's Snake", biomass carbon source and sucrose were used to fabricate Fe/Fe_3O_4@porous carbon (PC) composite materials through combustion experiments. Subsequently, high-temperature calcination was applied to enhance the microwave absorbing properties of the materials. The as-prepared composites demonstrate an impressive 6.62 GHz effective bandwidth and an excellent absorption ability of −51.54 dB at a matched thickness of 2.2 mm. Moreover, by tuning the content of magnetic particles and controlling the thickness of the composite material, comprehensive coverage across *C*, *X*, and *Ku* bands can be achieved. The outstanding performance suggests that the synthesized Fe/Fe_3O_4@PC porous materials hold significant potential for applications in electromagnetic wave absorption. It opens up a novel, straightforward, and cost-effective approach to acquiring broadband absorbing materials.

1. Introduction

In the ever-evolving landscape of scientific and technological advancements, the indubitable presence of electronic equipment has integrated into every aspect of our daily life. Meanwhile, the electromagnetic radiation and interference generated during the operation of electronic equipment will affect production and life, leading to the deterioration of the living environment [1–4]. Therefore, the development of a new type of electromagnetic absorbing material that uses green, renewable, and sustainable energy and technology has become imperative. Traditional absorbing materials have several drawbacks, including high density, low bandwidth, and large volume. Ideally, an excellent microwave absorber should be content with the characteristics of high efficiency, broad bandwidth and light weight as much as possible [5,6]. Thus, a simple and feasible method for preparing microwave-absorbing composites is necessary.

To overcome the limitations of traditional microwave-absorbing materials, novel materials have been explored by researchers, such as carbonaceous material [7,8], ferromagnetic material [9,10]. However, when used alone, the impedance matching and attenuation characteristic are not satisfactory [11,12]. Carbon-based microwave absorbing materials have unique advantages, including good thermal stability, low price, controllable microstructure [13]. In recent years, biomass carbon source has attracted the attention of researchers as a high-quality absorbing matrix. Sucrose, a common natural biomass carbon source, has the advantages of easy availability, biodegradability, and low cost [14]. It can be easily prepared into porous carbon materials through the "Pharaoh's Snake" experiment. Porous carbon with abundant mesopores and macropores structure have garnered attention, owing to their remarkable potential in diminishing interface reflections and facilitating

* Corresponding author at: Hubei Key Laboratory for New Textile Materials and Applications, School of Materials Science and Engineering, Wuhan Textile University, Wuhan 430200, China.
** Corresponding author.
E-mail addresses: whutfrpzhangbin@163.com (B. Zhang), quzhengyao@whut.edu.cn (Z. Qu).

https://doi.org/10.1016/j.jallcom.2024.174402
Received 9 January 2024; Received in revised form 10 March 2024; Accepted 3 April 2024
Available online 4 April 2024

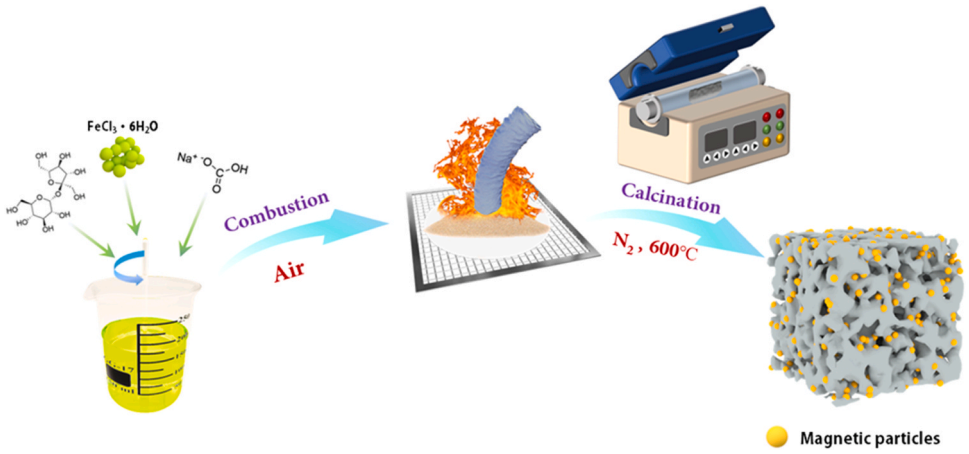

Scheme 1. Flowchart for the synthesis process of Fe/Fe_3O_4@PC composite materials.

impedance matching. Diverse configurations of porosity, including microporous, concave, and hollow-bowl structures, exhibit the ability to induce multiple reflections and attenuations, thereby enabling efficient electromagnetic absorption [15]. Furthermore, the inherent porosity contributes to reducing weight and density, rendering them immensely desirable as absorbers.

According to the absorption theory, the intricate interplay between the dielectric loss and magnetic loss profoundly influences absorbing performance [16,17]. Incorporating magnetic components into carbon materials can resolve the challenge of inadequate microwave absorption performance resulting from the use of single-component materials [18,19]. Single-component dielectric materials typically possess high dielectric constant and low magnetic permeability. The addition of magnetic materials can assist in enhancing impedance matching [20]. Their combination creates a synergistic effect that enhances microwave absorption properties. For example, Lu et al. [21] conducted a study on porous Co/C nanocomposites, utilizing controlled atmospheres and thermal decomposition of metal-organic framework materials, which exhibited excellent reflection loss (RL) of −35.30 dB and a broad absorption band (5.80 GHz). Li and coworkers [22] also prepared morphology-controlled porous Fe_3O_4 nanostructures, although their effective absorption bandwidth (EAB) was only 2.56 GHz. Wu et al. [23] synthesized three-dimensional porous Fe_3O_4/C composite flowers through a solvothermal and carbon reduction process, with an RL_{min} of −54.60 dB and an absorption bandwidth of 6.00 GHz. Xie et al. [24] prepared lightweight PC/Fe_3O_4@PDA hybrid nanocomposites using a combination of carbonization, hydrothermal treatment and self-polymerization, which showed a minimal RL value of −46.67 dB. The preparation of the porous structure described above can be a complex and energy-intensive process when using custom equipment. Concurrently, challenges with impedance matching may arise, making it crucial to develop a method with facile operation and efficient synthesis.

Herein, inspired by the "Pharaoh's Snake" experiment, Fe/Fe_3O_4@porous carbon composites were synthesized as effective microwave absorbers. By adjusting the content of magnetic particles, we can achieve controllable changes in the electromagnetic parameters of the composites. However, the as-prepared composite has a relatively low dielectric constant (Fig. S1, Supplementary Material), which hinders the absorption of EMW. High-temperature calcination under protective gas has been reported to enhance the absorption performance [25]. As anticipated, the prepared lightweight Fe/Fe_3O_4@PC composite (Fig. S5, Supplementary Material) achieves a wider bandwidth and adjustable absorbing performance.

2. Experimental section

2.1. Materials

Sinopharm Chemical Regent Co., Ltd. provided ferric chloride hexahydrate ($FeCl_3$·$6H_2O$, 99 %), ethanol (99.7 %) and paraffin wax. Sucrose (99 %) and sodium bicarbonate ($NaHCO_3$, 99 %) were received from Chengdu Kelong Chemical Co., Ltd. All chemicals utilized in this investigation were of analytical grade and were employed without any additional purification.

2.2. Preparation of Fe/Fe_3O_4@PC composites

Dissolved $FeCl_3$·6 H_2O (1.2/2.4/3.6/4.8/6.0 g) in 40 ml of alcohol with ultrasonic agitation for about 30 s. Measured 16 g of sucrose and 4 g of $NaHCO_3$, then add them to the $FeCl_3$·6 H_2O solution. Thoroughly stirred the mixture and then lighted it. The combustion experiment was conducted in a well-ventilated environment, after the complete reaction, Fe_3O_4@PC composites absorbing material was obtained (the growth process of porous material is shown in **video S1**). The mass ratio of magnetic nanoparticles can effectively control the EMW absorption performance. Subsequently, the material was calcined at 600 ℃ for 2 h under a N_2 atmosphere. Fe/Fe_3O_4@PC composites materials with remarkable absorption properties were prepared. The synthesized products were denoted as FPC-0, FPC-2, FPC-4, FPC-6, FPC-8 and FPC-10, based on the mass fraction of Fe/Fe_3O_4 particles. The fabrication process of Fe/Fe_3O_4@PC nanocomposite is illustrated in Scheme 1.

Supplementary material related to this article can be found online at doi:10.1016/j.jallcom.2024.174402.

2.3. Characterization

The porous structure and the morphology of magnetic particles attached to carbon were observed using scanning electron microscope (SEM, Zeiss Sigma 300) at different magnifications. Energy-dispersive spectroscopy (EDS, Oxford X-MAX), X-ray diffraction (XRD, D8 Advance and DAVINCI DESIGN) and X-ray photoelectron spectroscopy (XPS, Thermo Scientific Escalab 250Xi) were used to analyze the chemical composition, chemical bonds, and crystal phase information. The BET test was employed to analyze the N_2 adsorption-desorption curves of the Fe/Fe_3O_4@PC composite and determine the specific surface area (S_{BET}) and pore diameter. The hysteresis curves and magnetic properties of Fe/Fe_3O_4@PC composites were evaluated by a vibrating sample magnetometer (VSM, Lake Shore 7037). Electromagnetic wave absorption performance testing was conducted within a frequency range of 2 GHz to 18 GHz using the coaxial method, employing the vector network analyzer (VNA, China Electronics Technology Instruments Co.,

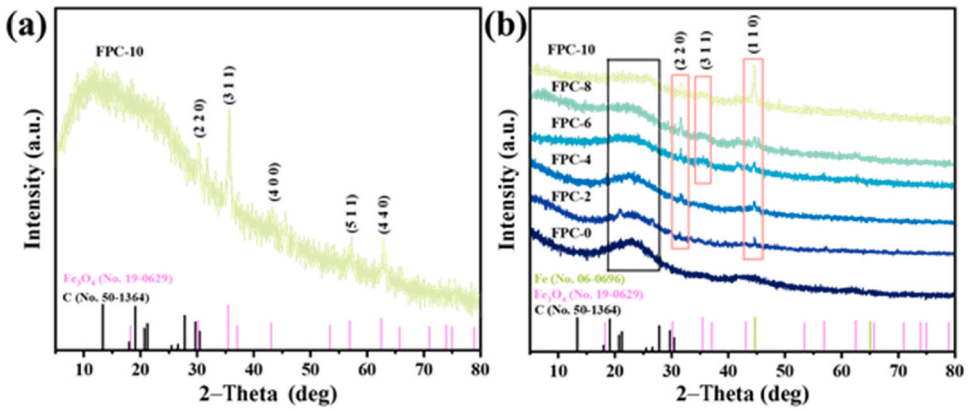

Fig. 1. (a) XRD patterns of FPC-10 samples that have not been calcined at high temperature. (b) XRD patterns of the Fe/Fe_3O_4@PC nanocomposites.

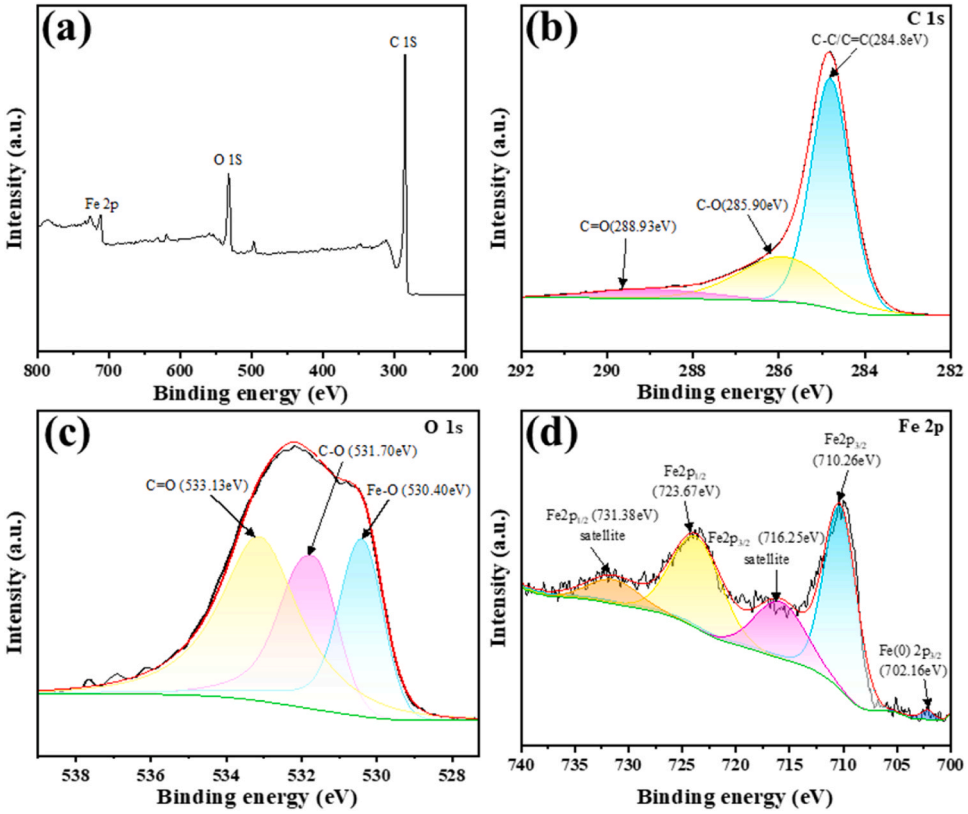

Fig. 2. (a) XPS survey spectrum of the FPC-10 sample. (b) C 1 s. (c) O 1 s. (d) Fe 2p.

Ltd 3672 C). The Fe/Fe_3O_4@PC nanocomposite was mixed with paraffin at a doping ratio of 2:3 at 180 °C and compressed into a ring shape (Φ_{in} = 3.04 mm, Φ_{out} = 7.00 mm).

3. Results and discussion

Fig. 1 illustrates the XRD patterns of synthetic absorbing materials. It is evident that a broad and weak diffraction peak is observed around 2θ about 20–30°, indicative of a typical amorphous carbon structure. It is worth noting that Fig. 1a represents the spectrum of the FPC-10 sample that has not undergone calcination. In this sample, five characteristic peaks corresponding to the (2 2 0), (3 1 1), (4 0 0), (5 1 1) and (4 4 0) planes of spinel-type ferrite (JCPDS No. 19–0629) are observed at angles of 30.09°, 35.42°, 43.05°, 57.27° and 62.52°, respectively [26]. The carbonized material (Fig. 1b) exhibits a sharp absorption peak at 44.56°, which matches the (1 1 0) crystal plane of Fe (JCPDS No. 06–0696). Additionally, a weaker diffraction peak is observed at 35.42° can be referred to the (3 1 1) crystal plane of ferrite, suggesting the occurrence of C-catalyzed reduction of ferrite during the carbonization process [27, 28]. Moreover, as the Fe^{3+} concentration increases, the magnitude of the diffraction peaks of iron and ferrite also increases, while the C signal shows the opposite trend. It is ascribed to the intercalation of Fe/Fe_3O_4 particles, preventing the agglomeration and re-accumulation of porous carbon and facilitating the decoration of a higher number of magnetic particles.

Fig. 2a displays the XPS wide spectrum of representative FPC-10 sample, wherein the three characteristic peaks correspond to the elements of C, Fe and O. The C 1 s spectrum is shown in Fig. 2b, revealing distinctive peaks at 284.80 eV, 285.90 eV and 288.93 eV, which can be attributed to C-C/C═C, C-O and C═O bonds, separately [29]. The O 1 s

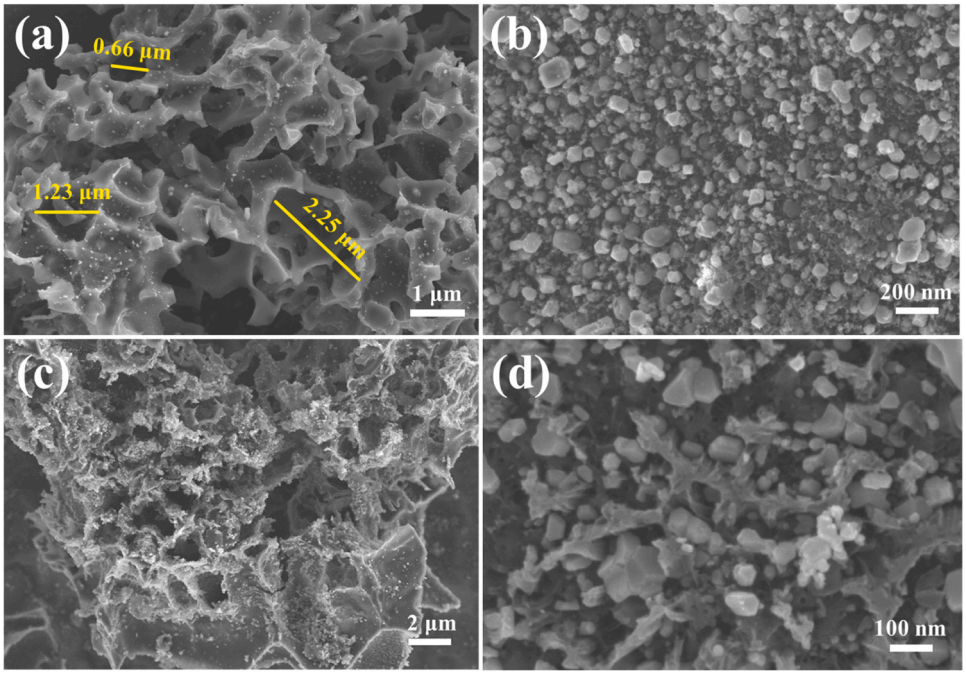

Fig. 3. SEM images of (a) porous structure; (b), (c) and (d) the specimen after doping magnetic particles.

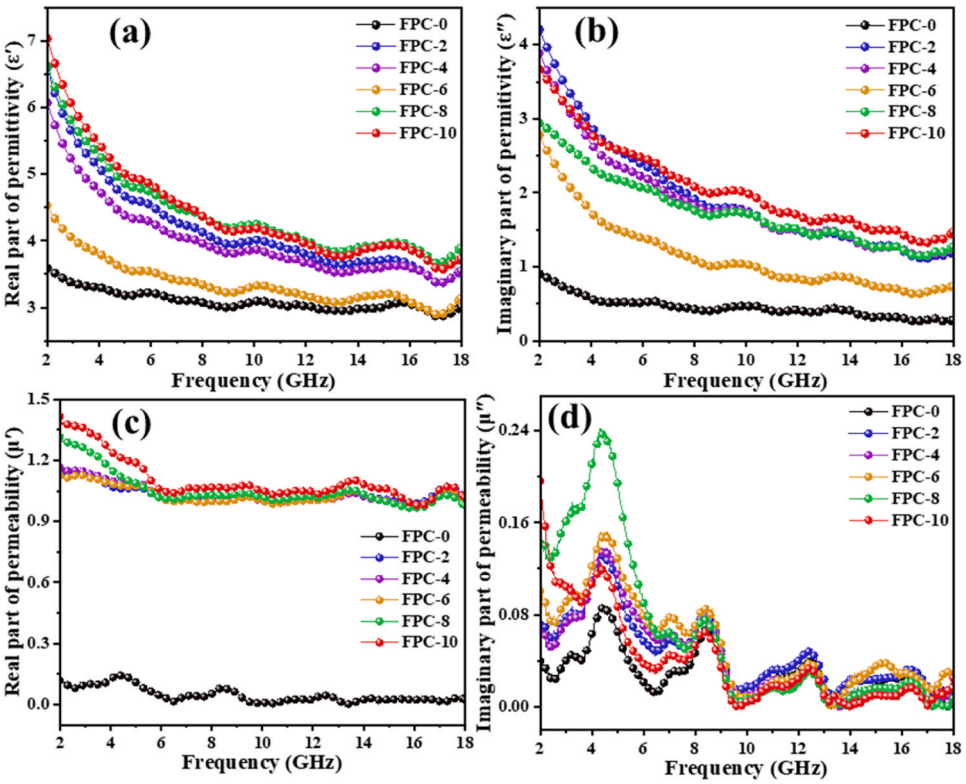

Fig. 4. The variations in (a) ε', (b) ε'', (c) μ' and (d) μ'' with different Fe^{3+} loading rates.

pattern (Fig. 2c) displays three peaks, with those appearing at 533.13 eV and 531.70 eV associated with O-C═O and C-O functional groups. The split peak at 530.40 eV is associated with the metal-oxygen bond, indicating the fixation of magnetic nanoparticles on the PC surface through Fe-O bond [30]. The Fe 2p spectrum (Fig. 2d) reveals a broad peak at 702.16 eV, attributed to the elemental Fe. Peaks at 710.26 eV and 723.67 eV correspond to Fe $2p_{3/2}$ and Fe $2p_{1/2}$, respectively, suggesting the existence of multivalent iron ions (Fe^{2+} and Fe^{3+}) in the sample. In addition, the faint peaks at 716.25 eV and 731.38 eV correlate with the ferrite satellite peak [4,31].

Fig. 3a exhibits low-magnification image of FPC-0, demonstrating abundant porous structures with pore diameters ranging from 0.5 to 2.75 μm. In addition, the structure of FPC-10 is analyzed using N_2 adsorption–desorption isotherms (Fig. S2, Supplementary Material),

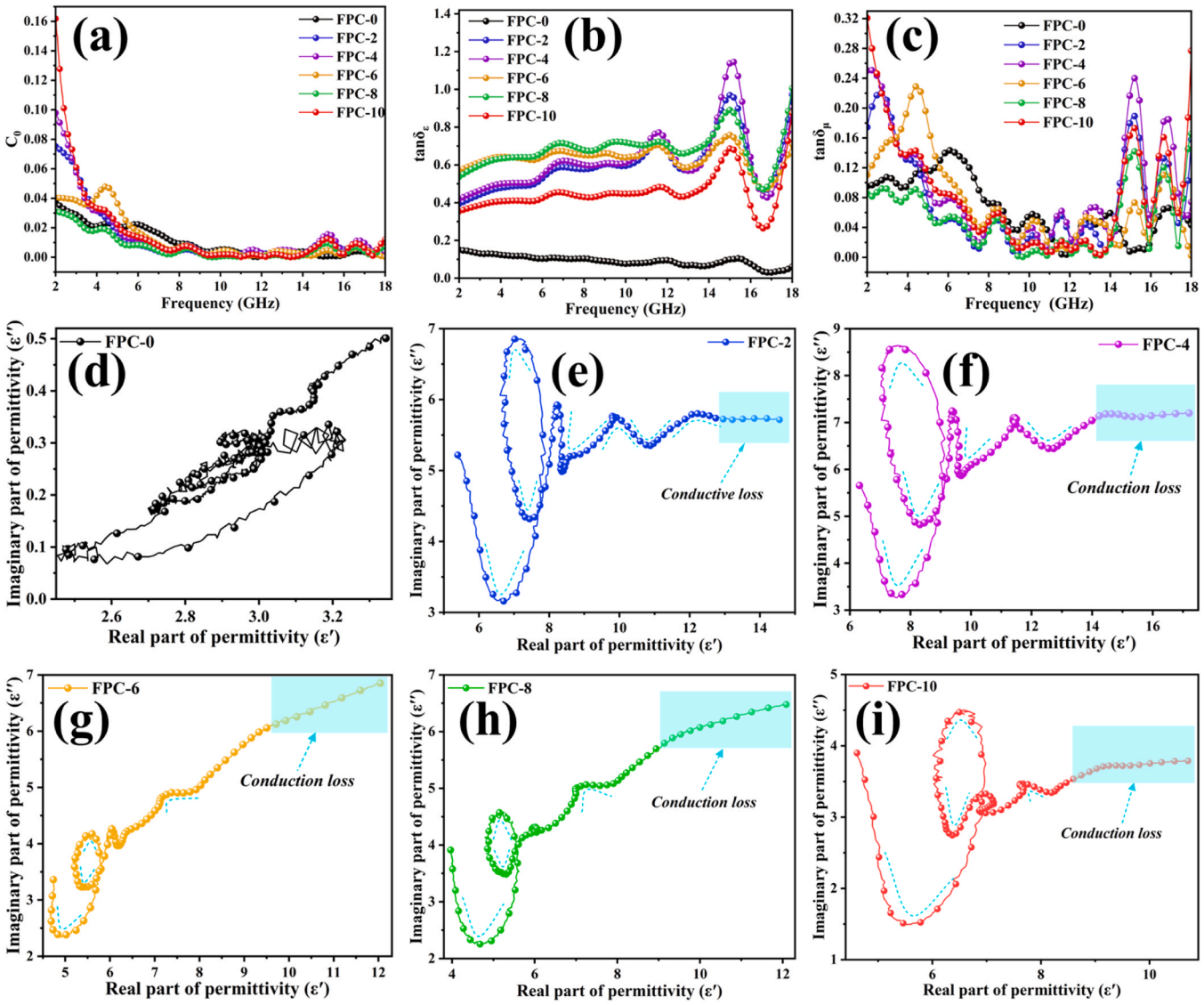

Fig. 5. (a) The C_0-f curves of Fe/Fe_3O_4@PC composites; (b) and (c) $tan\delta_\varepsilon$ and $tan\delta_\mu$ of all samples with different Fe^{3+} loading rates; (d) Cole-Cole curves of all samples.

revealing the irreversible adsorption phenomenon. It is obvious that the S_{BET} measures 310.81 $m^2 \cdot g^{-1}$, and the average pore diameter is 4.60 nm using the BJH method. These porous structures not only contribute to lightweight reduction but also provide multiple scattering and reflection capabilities for incident EMW, aiding in the modulation of absorption properties. In addition, the dielectric properties of the material can also be improved. With an increase in Fe^{3+} content, numerous small magnetic particles can be observed densely aggregated on the surface of porous carbon in Fig. 3b. At higher magnifications (Fig. 3c, d), the uniform dispersion of Fe/Fe_3O_4 on the material surface is evident, displaying a spherical or granular morphology. Fig. S3 (as shown in Supplementary Material) depicts the distribution of C, O and Fe captured from specific regions of the Fe/Fe_3O_4@PC nanocomposites, confirming the presence of carbon framework and Fe/Fe_3O_4 nanospheres. The above-mentioned tests confirm the successful synthesis of the Fe/Fe_3O_4@PC material.

To assess the absorption capabilities of Fe/Fe_3O_4@PC composites, an analysis of the complex permittivity ($\varepsilon_r = \varepsilon' - j\varepsilon''$) and complex permeability ($\mu_r = \mu' - j\mu''$) is conducted. Fig. 4a-b show the ε' value of composites decrease from 17.20 to 2.74, while the ε'' value range from 8.64 to 0.07. The composites containing Fe and Fe_3O_4 exhibit remarkable dielectric properties. Interestingly, the ε' value reduces overall within the range of 2–18 GHz, a phenomenon known as the frequency dispersion effect is commonly observed in composite materials comprising carbon and magnetic components [27,32], favoring EMW attenuation. On the other hand, the ε''-f curve appears a resonance peak in the 8–18 GHz range. The polarization process within the composite material may lag behind the changes in the external alternating electromagnetic field at higher frequency, thereby failing to achieve immediate stability and resulting in fluctuations [33]. The presence of resonance peaks indicates that the samples have a certain polarization relaxation behavior in the external electric field, leading to energy dissipation of the EMW. Besides, Fig. 4a displays that the FPC-4 sample has the highest ε_r value, suggesting that a higher content of magnetic particles does not lead to improved dielectric performance. According to the reported literature, conductivity and polarization are the primary factors influencing the permittivity value [26]. Increasing the content of magnetic material enhances the synergistic effect between the components, thereby improving conductivity of carbon and the dielectric properties of the composite. Carbon catalytically reduces Fe^{3+} and Fe^{2+} at high temperature to obtain elemental Fe, forming Fe/Fe_3O_4 core. In addition, the interfacial interaction between the magnetic particles and carbon

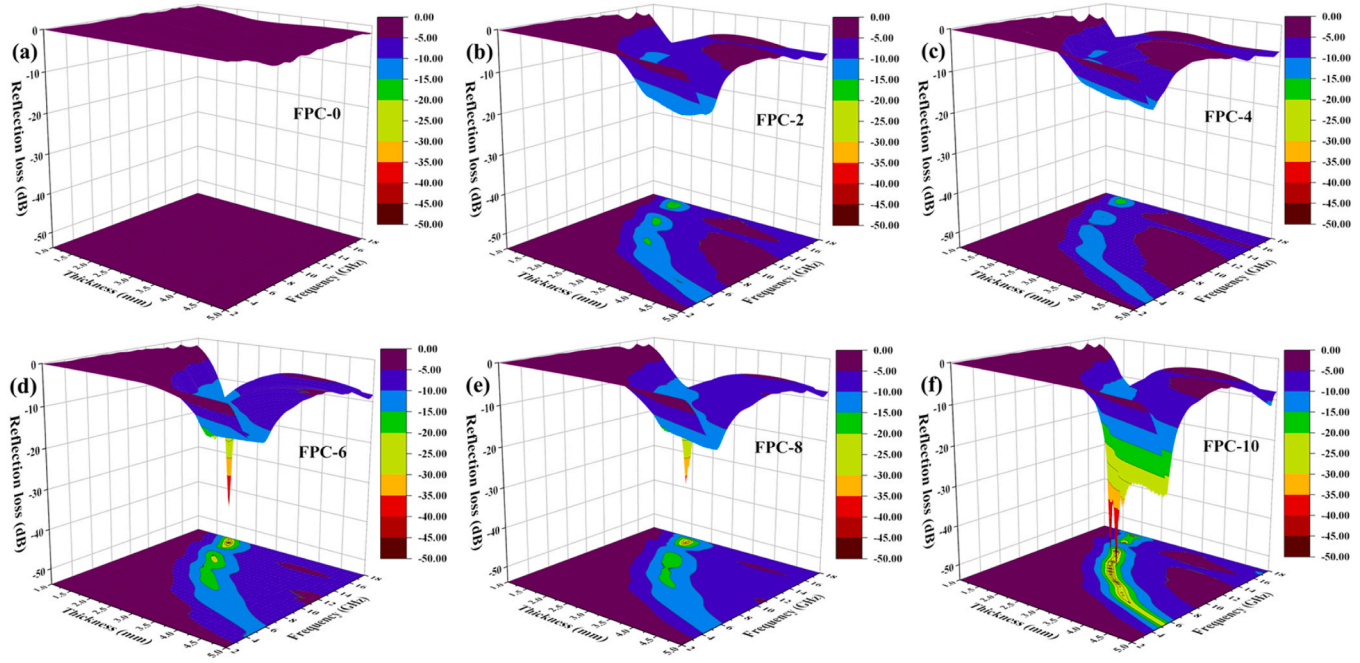

Fig. 6. 3D reflection loss graphe of the Fe/Fe_3O_4@PC composite materials (a) FPC-0, (b) FPC-2, (c) FPC-4, (d) FPC-6, (e) FPC-8 and (f) FPC-10.

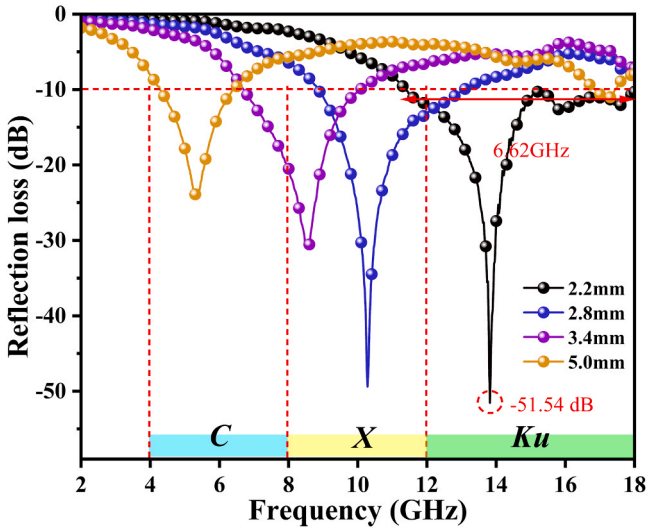

Fig. 7. Reflection loss of FPC-10 sample with given thickness of 2.2 mm, 2.8 mm, 3.4 mm and 5.0 mm.

establishes a conductive pathway, reducing electron scattering at the interface and enhancing the conductivity of Fe/Fe_3O_4@PC composites [34]. However, higher Fe/Fe_3O_4 content will result in a thicker shell in the composite material. It inhibits electron migration among the porous carbon particles, resulting in decreased conductivity for FPC-6, FPC-8, and FPC-10 samples, along with a reduction in the dielectric constant [35,36].

The real part (μ') remains below 1.4, whereas the imaginary part (μ'') maintains relatively low levels across the frequency of 2–18 GHz (Fig. 4c-d). Although the permeability constant is lower compared to the permittivity, the synergistic interaction between magnetic and nonmagnetic components influences the overall EMW dissipation performance. Magnetic loss can beprimarily classified into three categories: hysteresis loss, eddy current loss and magnetic resonance loss [37,38]. The closed area of the hysteresis loop of the composite with added

Table 1
Comparison of EMW absorption of some absorbers reported in earlier studies.

Absorber	Thickness (mm)	RL_{min} (dB)	EAB (GHz)	Ref.
3DC/Fe_3O_4	3.0	-37.8	5.95	[46]
HPC/Fe_3O_4	5.5	-20.1	unknow	[47]
Fe_3O_4/carbon foams	1.9	-47.3	5.68	[30]
$HcFe_3O_4$@C	3.5	-46.3	5.04	[48]
Porous Fe_3O_4/C	2.1	-22.2	6.0	[23]
Fe_3O_4/C composites	2.5	-18.73	5.4	[16]
FPC-6	2.3	-21.58	7.02	This work
FPC-8	2.4	-19.4	7.1	This work
FPC-10	2.2	-51.54	6.62	This work

magnetic particles is notably larger than that of FPC-0 (Fig. S4, Supplementary Material), indicating that the introduction of Fe/Fe_3O_4 particles increases hysteresis loss and enhances the absorption of EMW. The calculation of eddy current loss is based on the measured parameters of μ' and μ''. If $C_0 = \mu''(\mu')^{-2}f^{-1}$ [39] remains constant, eddy current loss becomes the dominant contributor to magnetic loss [40]. For Fig. 5a, the C_0 value of the Fe/Fe_3O_4@PC composite decreases significantly in the 2–8 GHz range, and some resonance peaks appear. This suggests that natural resonance predominates as the magnetic loss mechanism in low-frequency environments [41]. After that, the value of C_0 tends to be stable, which implies that eddy current loss becomes the main mechanism of magnetic loss. Furthermore, the resonance peaks of Fe/Fe_3O_4@PC around 15 GHz and 16.5 GHz are attributed to the exchange resonance induced by the doping of Fe/Fe_3O_4 particles.

Dielectric loss and magnetic loss are widely recognized as the two fundamental mechanisms responsible for attenuating EMW [29]. Fig. 5b-c depict the variation of dielectric loss tangent ($tan\delta_\varepsilon = \varepsilon''/\varepsilon'$) and magnetic loss tangent ($tan\delta_\mu = \mu''/\mu'$) with frequency. Notably, the $tan\delta_\varepsilon$ values for the samples consistently exceed their $tan\delta_\mu$ values. This difference can be attributed to the fact that the only components in the

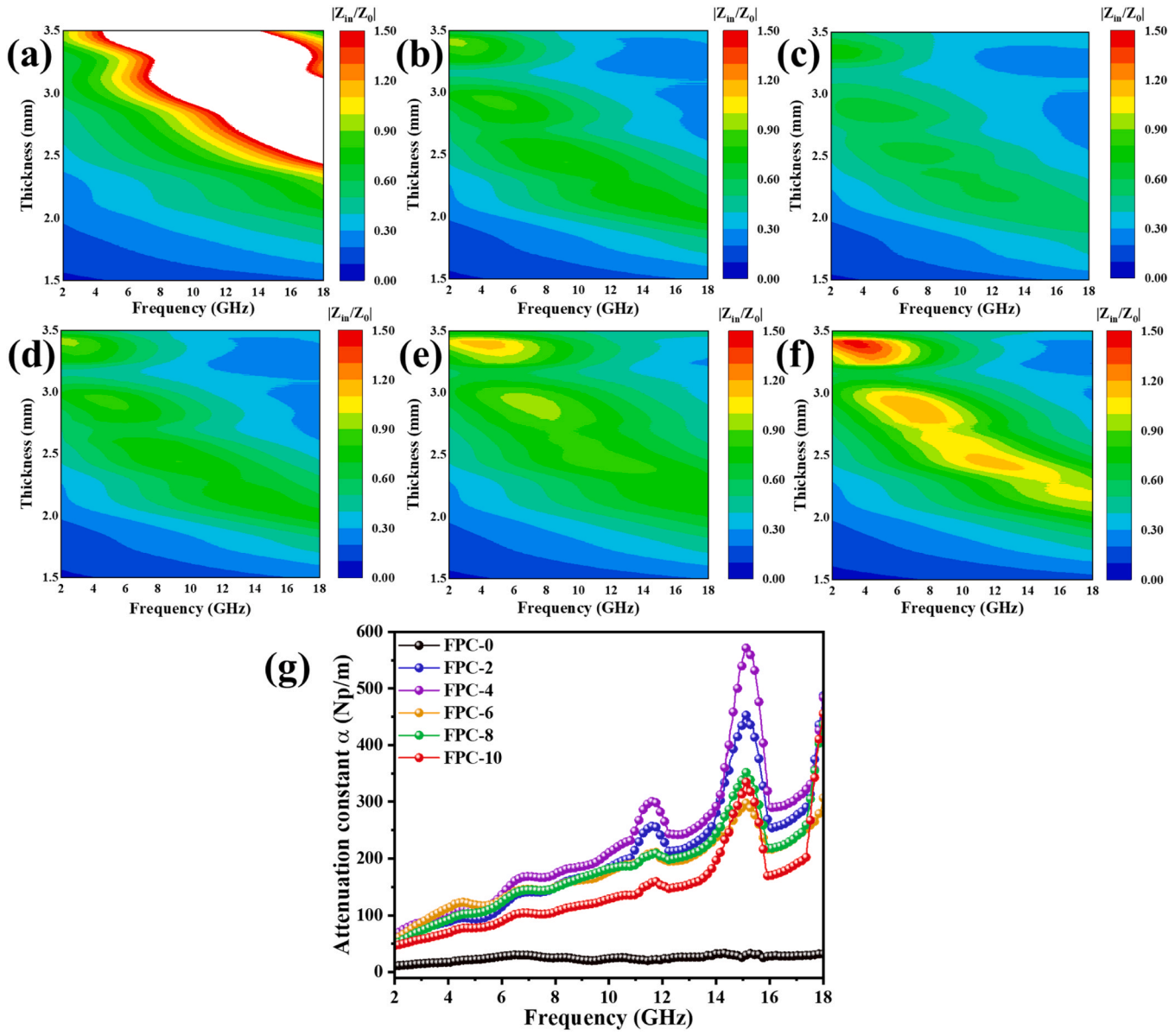

Fig. 8. Impedance matching diagrams of samples (1.5–3.5 mm): (a) FPC-0, (b) FPC-2, (c) FPC-4, (d) FPC-6, (e) FPC-8, (f) FPC-10. (g) attenuation constant (α) of all samples.

composite that produce magnetic loss are nano-Fe/Fe_3O_4 particles, whereas both porous carbon and ferrite contribute to dielectric loss. Moreover, the formation of porous structures and heterogeneous interfaces can induce interfacial polarization, improving the dielectric loss. Therefore, we can infer that dielectric loss constitutes the primary factor contributing to the attenuation of EMW.

According to Debye theory, polarization relaxation can be described by the Cole–Cole curve, which is commonly derived from the subsequent equation [42]:

$$\left(\varepsilon' - \frac{\varepsilon_s + \varepsilon_\infty}{2}\right)^2 + (\varepsilon'')^2 = \left(\frac{\varepsilon_s - \varepsilon_\infty}{2}\right)^2 \quad (1)$$

where ε_s, ε_∞ represent the static permittivity and the relative permittivity at high frequency, seperately. Each semicircle represents a relaxation process [43]. Fig. 5d-i display the Cole-Cole plots of all samples. The material doped with Fe/Fe_3O_4 nanoparticles exhibits approximately six irregular semicircles, indicating the occurrence of polarization relaxation phenomena. It is attributed to the embedding of magnetic particles, which fosters the formation of heterogeneous interfaces. Consequently, this enhances interface polarization and also induces a dipolar polarization effect [36]. Furthermore, with the content of magnetic particles rises, the Cole curve demonstrates a linear trend under high-frequency conditions, accompanied by an increase in tail length, signifying heightened conduction loss. It is primarily due to the increased degree of graphitization [34].

To further investigate the absorption properties of the materials, simulated calculations of the RL values at various thicknesses are performed. These calculations are based on the formula [44,45]:

$$RL = 20log|(Z_{in} - Z_0)/(Z_{in} + Z_0)| \quad (2)$$

$$Z_{in} = \sqrt{\mu_r/\varepsilon_r}\tanh\left(j2\pi fd\sqrt{\mu_r\varepsilon_r}/c\right) \quad (3)$$

Where Z_0 is the free space impedance, Z_{in} denotes for intrinsic impedance, and d is given thickness from 1 mm to 5 mm, c is the light speed. When RL measures below −10 dB, it indicates that more than 90 % of the EMW entering the absorber have been effectively absorbed. Fig. 6 presents the three-dimensional RL curves of composites across a frequency range spanning from 2 to 18 GHz. Clearly, the FPC-0 sample has

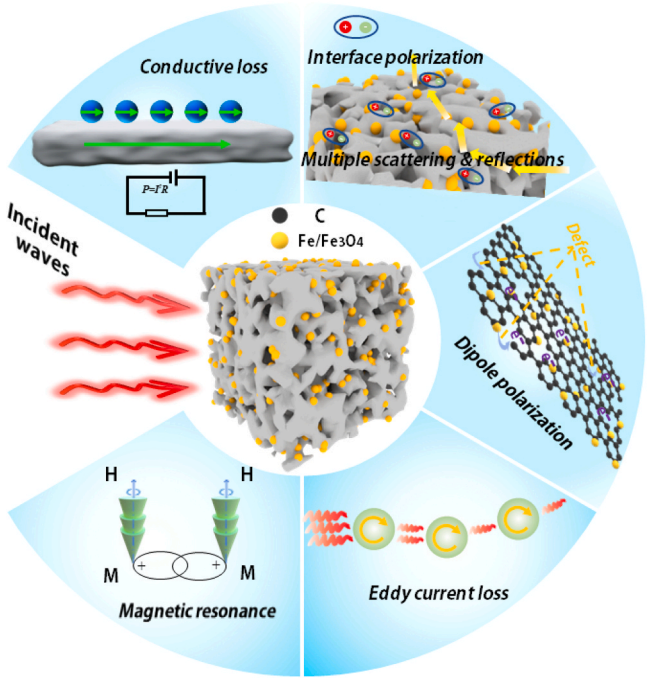

Scheme 2. EMW absorption mechanisms of Fe/Fe_3O_4@PC composites.

no effective absorption across all bands. In contrast, the incorporation of magnetic particles into the porous carbon structure enables effective absorption. FPC-2 and FPC-4 demonstrate RL_{min} values of −20.82 dB and −19.28 dB, respectively, with an EAB of approximately 2 GHz. The FPC-6 sample achieves an RL value of −21.58 dB, with an absorption bandwidth spanning 7.02 GHz (10.98–18 GHz). Despite the RL_{min} value of the FPC-8 sample being only −19.4 dB, it demonstrates the widest EAB of 7.10 GHz ($d = 2.4$ mm), effectively covering the entire *Ku* band and the most of *X*-band. This phenomenon is attributed to the uniform distribution of Fe/Fe_3O_4 nanospheres on the porous carbon surface without the occurrence of "dead zones", resulting in heightened magnetic loss and enhanced interfacial polarization. However, the FPC-10 sample shows the lowest RL value of −51.54 dB at 13.82 GHz, with a matching thickness of 2.2 mm and an EAB of 6.62 GHz (11.38–18 GHz), exhibiting excellent microwave absorption performance. Besides, an increase in the thickness of the composites results in a reduction of the frequency obtaining RL_{min}. Fig. 7 illustrates that adjusting the thickness facilitates the easy attainment of an effective bandwidth covering the *X*-band and *C*-band. Therefore, achieving optimal absorption performance entails manipulating material parameters and carefully selecting the appropriate thickness. A detailed comparison between the Fe/Fe_3O_4@PC microspheres and other previously reported absorbers coated with magnetic particle is presented in Table 1, suggesting that the samples exhibit good absorption properties.

In order to achieve efficient absorption of EMW, two simultaneous requirements must be satisfied: excellent impedance matching and attenuation characteristics. The formula for calculating the attenuation constant α is as follows [49]:

$$\alpha = \frac{\pi f}{c}\left(2(\mu''\varepsilon'' - \mu'\varepsilon') + \left((\mu''^2 + \mu'^2)(\varepsilon''^2 + \varepsilon'^2)^{\frac{1}{2}}\right)\right)^{\frac{1}{2}} \quad (4)$$

Generally speaking, a larger attenuation constant α indicates a stronger attenuation ability of EMW and improves the absorption performance. Additionally, an impedance matching value closer to 1 signifies better impedance matching, allowing for more efficient penetration of EMW into the absorbing material. The value of $|Z_{in}/Z_0|$ calculated using Eq. (3) exhibits a similar trend for samples incorporating magnetic nanoparticles (Fig. 8a-f) [50]. However, the FPC-0 sample comprised entirely of pure dielectric porous carbon, demonstrates poor impedance. It is worth noting that the impedance matching value of the FPC-10 sample is closer to 1. Consequently, a greater of electromagnetic waves can penetrate absorbing materials, leading to a broader effective absorption bandwidth. The calculated attenuation constant α (Fig. 8g) demonstrates that FPC-10 has the lowest value, albeit still considerably higher than FPC-0. Based on the above analysis, FPC-10 demonstrates the most desirable electromagnetic absorption performance. This outatanding performance is attributed to several factors: (1) the interface between Fe/Fe_3O_4 magnetic particles and porous carbon, along with the rich porous structure, facilitates multiple reflections and absorptions of EMW. It induces the interface polarization effect, significantly enhancing the EMW absorption capacity. (2) Both porous carbon and Fe/Fe_3O_4 magnetic particles in the composite material have certain dielectric properties. Under the influence of external electric fields, internal electrons occur transitions, resulting in conductive loss. (3) The dispersion of a large number of Fe/Fe_3O_4 particles within the porous carbon leads to dipole polarization effects, causing dipole polarization loss, which further enhances EMW absorption. (4) The introduction of magnetic particles not only improves the impedance matching of the material but also produces magnetic loss, as depicted in Scheme 2 [51,52].

4. Conclusion

In summary, Fe/Fe_3O_4@PC composites were synthesized to function as effective microwave absorbers, drawing inspiration from the ''Pharaoh's Snake'' experiment. It exhibited excellent electromagnetic absorption properties through precise manipulation of the filling content of Fe/ Fe_3O_4 magnetic particles. The FPC-10 sample has an RL value of −51.54 dB at a thickness of 2.2 mm, and its EAB has also reached 6.62 GHz, encompassing the entire *Ku*-band and a substantial portion of the *X*-band. These outstanding features can be attributed to the intricate interplay between the diverse porous structure, magnetic resonance phenomena, and multiple absorption mechanisms. Consequently, Fe/Fe_3O_4@PC composites can find broad applications in the field of microwave absorption, and a method for crafting lightweight porous carbon/magnetic composites displaying exceptional absorption characteristics is proposed.

CRediT authorship contribution statement

Heng Yang: Writing – review & editing, Writing – original draft, Software, Methodology, Investigation, Formal analysis. **Xin Jiang:** Methodology, Investigation. **Jiuxiao Sun:** Methodology, Funding acquisition. **Bin Zhang:** Conceptualization, Funding acquisition, Supervision, Writing – review & editing. **Xiaogang Su:** Investigation. **Qilei Wu:** Software, Validation. **Zhengyao Qu:** Supervision, Writing – review & editing. **Siqi Huo:** Writing – review & editing.

Declaration of Competing Interest

The authors declare that they have no known competing financial interests or personal relationships that could have appeared to influence the work reported in this paper.

Data Availability

The data that has been used is confidential.

Acknowledgments

This work was supported by Hubei Key Laboratory for New Textile Materials and Applications (FZXCL202208); the Hubei Key Laboratory of Digital Textile Equipment (DTL2020014); the Hubei Longzhong Laboratory (2022KF-02); and the Hubei provincial Technical Research

Project (JD2023009).

Appendix A. Supporting information

Supplementary data associated with this article can be found in the online version at doi:10.1016/j.jallcom.2024.174402.

References

[1] M. Sun, Z. Xiong, Z. Zhang, C. Chen, L. Qin, D. Wang, F. Wu, P. Liu, One-dimensional Ag@NC-Co@NC composites with multiphase core-shell hetero-interfaces for boosting microwave absorption, Compos. Sci. Technol. 228 (2022) 109663.

[2] M. Wu, L. Rao, Y. Li, Z. Ji, L. Liu, P. Wang, G. Ying, Urchin-like Fe3O4@C with core-shell structure modified 2D MXene for high-performance microwave absorption, J. Alloy. Compd. 971 (2024) 172552.

[3] Y. Zhang, S. Gao, J. He, F. Wei, X. Zhang, CoFe@C composites decorated with residual carbon as an ultrathin microwave absorber in the X and Ku bands, Diam. Relat. Mater. 141 (2024) 110666.

[4] S. Gao, Y. Zhang, J. He, X. Zhang, F. Jiao, T. Liu, H. Li, C. Wu, M. Ma, Coal gasification fine slag residual carbon decorated with hollow-spherical Fe3O4 nanoparticles for microwave absorption, Ceram. Int. 49 (2023) 17554–17565.

[5] W. Wang, X. Deng, D. Liu, F. Luo, H. Cheng, T. Cao, Y. Li, Y. Deng, W. Xie, Broadband radar-absorbing performance of square-hole structure, Adv. Compos. Hybrid. Mater. 5 (2022) 525–535.

[6] M. Fu, H. Yu, W. Chen, Construction of Co3O4 porous rod/graphene heterostructures toward strong and broadband microwave absorption applications, Appl. Surf. Sci. 622 (2023) 156946.

[7] Y. He, Y. Liu, X. Yan, G. Qin, Y. Liu, B. Zhong, L. Xia, D. Liu, Y. Zhou, X. Huang, Mesoscopically ordered Fe3O4/C nano-composite for superior broadband electromagnetic wave absorption, Compos. Part A: Appl. Sci. Manuf. 158 (2022) 106983.

[8] P. Han, C. Wu, J. Tai, H. Zhang, G. Zhao, Q. Chen, Y. Liu, Improved microwave absorption properties of ferrite-rGO composites by covalent bond, J. Alloy. Compd. 966 (2023) 171581.

[9] T. Hou, Z. Jia, B. Wang, H. Li, X. Liu, L. Bi, G. Wu, MXene-based accordion 2D hybrid structure with Co9S8/C/Ti3C2Tx as efficient electromagnetic wave absorber, Chem. Eng. J. 414 (2021) 128875.

[10] Z. Gao, Y. Schwab, Y. Zhang, N. Song, X. Li, Ferromagnetic nanoparticle–assisted polysulfide trapping for enhanced lithium–sulfur batteries, Adv. Funct. Mater. 28 (2018) 1800563.

[11] Y. Chen, P. Pötschke, J. Pionteck, B. Voit, H. Qi, Multifunctional cellulose/rGO/Fe3O4 composite aerogels for electromagnetic interference shielding, ACS Appl. Mater. Interfaces 12 (2020) 22088–22098.

[12] J. He, S. Gao, Y. Zhang, X. Zhang, H. Li, N-doped residual carbon from coal gasification fine slag decorated with Fe3O4 nanoparticles for electromagnetic wave absorption, J. Mater. Sci. Technol. 104 (2022) 98–108.

[13] R. Shen, M. Weng, L. Zhang, J. Huang, X. Sheng, Biomass-based carbon aerogel/Fe3O4@PEG phase change composites with satisfactory electromagnetic interference shielding and multi-source driven thermal management in thermal energy storage, Compos. Part A: Appl. Sci. Manuf. 163 (2022) 107248.

[14] R. Narasimman, S. Vijayan, K.S. Dijith, K.P. Surendran, K. Prabhakaran, Carbon composite foams with improved strength and electromagnetic absorption from sucrose and multi-walled carbon nanotube, Mater. Chem. Phys. 181 (2016) 538–548.

[15] M. Liu, Y. Liu, H. Guo, B. Zhang, L. Ren, A. Bashir, S.-L. Bai, Y. Ge, A facile way to enhance microwave absorption properties of rGO and Fe3O4 based composites by multi-layered structure, Compos. Part A: Appl. Sci. Manuf. 146 (2021) 106411.

[16] X. Liu, Y. Ma, Q. Zhang, Z. Zheng, L.-S. Wang, D.-L. Peng, Facile synthesis of Fe3O4/C composites for broadband microwave absorption properties, Appl. Surf. Sci. 445 (2018) 82–88.

[17] S. Liu, J. Wang, B. Zhang, X. Su, X. Chen, Y. Chen, H. Yang, Q. Wu, S. Yang, Transformation of traditional carbon fibers from microwaves reflection to efficient absorption via carbon fiber microstructure modulation, Carbon (2024) 118802.

[18] H. Liang, H. Xing, M. Qin, H. Wu, Bamboo-like short carbon fibers@Fe3O4@phenolic resin and honeycomb-like short carbon fibers@Fe3O4@FeO composites as high-performance electromagnetic wave absorbing materials, Compos. Part A: Appl. Sci. Manuf. 135 (2020) 105959.

[19] Y. Cui, J. Ge, T. Ma, L. Liu, P. Ju, F. Meng, F. Wang, Enhanced electromagnetic wave absorption of Fe3O4@C derived from spindle-like MOF, Mater. Lett. 316 (2022) 132060.

[20] X. Shu, S. Wang, W. Wu, S. He, H. Ren, Y. Song, Z. Zhao, Polyaniline-based networks combined with Fe3O4 hollow spheres and carbon balls for excellent electromagnetic wave absorption, Ceram. Int. 48 (2022) 811–823.

[21] Y. Lu, Y. Wang, H. Li, Y. Lin, Z. Jiang, Z. Xie, Q. Kuang, L. Zheng, MOF-derived porous Co/C nanocomposites with excellent electromagnetic wave absorption properties, ACS Appl. Mater. Interfaces 7 (2015) 13604–13611.

[22] X. Li, B. Zhang, C. Ju, X. Han, Y. Du, P. Xu, Morphology-controlled synthesis and electromagnetic properties of porous fe3o4 nanostructures from iron alkoxide precursors, J. Phys. Chem. C. 115 (2011) 12350–12357.

[23] N. Wu, C. Liu, D. Xu, J. Liu, W. Liu, Q. Shao, Z. Guo, Enhanced electromagnetic wave absorption of three-dimensional porous Fe3O4/C composite flowers, ACS Sustain. Chem. Eng. 6 (2018) 12471–12480.

[24] Y. Xie, Y. Guo, T. Cheng, L. Zhao, T. Wang, A. Meng, M. Zhang, Z. Li, Efficient electromagnetic wave absorption performances dominated by exchanged resonance of lightweight PC/Fe3O4@PDA hybrid nanocomposite, Chem. Eng. J. 457 (2023).

[25] S. Gao, L. Chen, Y. Zhang, J. Shan, Fe nanoparticles decorated in residual carbon from coal gasification fine slag as an ultra-thin wideband microwave absorber, Compos. Sci. Technol. 213 (2021) 108921.

[26] L.L. Adebayo, H. Soleimani, B.H. Guan, N. yahya, A. Öchsner, M. Sabet, J.Y. Yusuf, H. Ali, A simple route to prepare Fe3O4@C microspheres as electromagnetic wave absorbing material, J. Mater. Res. Technol. 12 (2021) 1552–1563.

[27] J. Fang, T. Liu, Z. Chen, Y. Wang, W. Wei, X. Yue, Z. Jiang, A wormhole-like porous carbon/magnetic particles composite as an efficient broadband electromagnetic wave absorber, Nanoscale 8 (2016) 8899–8909.

[28] H. Wang, F. Meng, J. Li, T. Li, Z. Chen, H. Luo, Z. Zhou, Carbonized design of hierarchical porous carbon/Fe3O4@Fe derived from loofah sponge to achieve tunable high-performance microwave absorption, ACS Sustain. Chem. Eng. 6 (2018) 11801–11810.

[29] Q. Liu, X. Liu, H. Feng, H. Shui, R. Yu, Metal organic framework-derived Fe/carbon porous composite with low Fe content for lightweight and highly efficient electromagnetic wave absorber, Chem. Eng. J. 314 (2017) 320–327.

[30] X. Zhou, C. Zhang, M. Zhang, A. Feng, S. Qu, Y. Zhang, X. Liu, Z. Jia, G. Wu, Synthesis of Fe3O4/carbon foams composites with broadened bandwidth and excellent electromagnetic wave absorption performance, Compos. Part A: Appl. Sci. Manuf. 127 (2019) 105627.

[31] M.C. Biesinger, B.P. Payne, A.P. Grosvenor, L.W.M. Lau, A.R. Gerson, R.S.C. Smart, Resolving surface chemical states in XPS analysis of first row transition metals, oxides and hydroxides: Cr, Mn, Fe, Co and Ni, Appl. Surf. Sci. 257 (2011) 2717–2730.

[32] Z. Wu, C. Yao, Z. Meng, Y. Deng, Y. Wang, J. Liu, Y. Wang, H. Zhou, Biomass-derived crocodile skin-like porous carbon for high-performance microwave absorption, Adv. Sustain. Syst. 6 (2022) 2100454.

[33] Z. Wu, J. Chang, X. Guo, D. Niu, A. Ren, P. Li, H. Zhou, Honeycomb-like bamboo powders-derived porous carbon with low filler loading, high-performance microwave absorption, Carbon 215 (2023) 118415.

[34] X. Wang, P. Ou, Q. Zheng, L. Wang, W. Jiang, Embedding multiple magnetic components in carbon nanostructures via metal-oxo cluster precursor for high-efficiency low-/middle-frequency electromagnetic wave absorption, Small, n/a 2307473.

[35] F. Wang, Y. Liu, R. Feng, X. Wang, X. Han, Y. Du, A "Win–Win" Strategy to Modify Co/C foam with carbon microspheres for enhanced dielectric loss and microwave absorption characteristics, Small 19 (2023) 2303597.

[36] X. Zhu, Y. Dong, F. Pan, Z. Xiang, Z. Liu, B. Deng, X. Zhang, Z. Shi, W. Lu, Covalent organic framework-derived hollow core-shell Fe/Fe3O4@porous carbon composites with corrosion resistance for lightweight and efficient microwave absorption, Compos. Commun. 25 (2021) 100731.

[37] H.H. Nguyen, N. Tran, T.L. Phan, D.S. Yang, N.T. Dang, B.W. Lee, Electronic structure, and magnetic and microwave absorption properties of Co-doped SrFe12O19 hexaferrites, Ceram. Int. 46 (2020) 19506–19513.

[38] J. Qiu, T. Qiu, Fabrication and microwave absorption properties of magnetite nanoparticle–carbon nanotube–hollow carbon fiber composites, Carbon 81 (2015) 20–28.

[39] Y. Chen, R. Qiang, Y. Shao, X. Yang, Q. Ma, R. Xue, B. Chen, S. Feng, F. Ren, Y. Ding, L. Sun, Z. Guo, Z. Ma, Z. Liu, X. Chen, Fe3C/Fe implanted hierarchical porous carbon foams for lightweight and broadband microwave absorption, Diam. Relat. Mater. 142 (2024) 110738.

[40] H. Zheng, R. Li, S. Dong, W. Chen, L. Fan, W. Li, P. Zheng, L. Zheng, Y. Zhang, L. Deng, Iron carbide interface modulating for synergies of 3D-graphene-like and iron-coated Fe3O4 particles for high microwave absorption performance, J. Alloy. Compd. 945 (2023) 169283.

[41] X. Guo, Z. Wu, J. Chang, D. Niu, A. Ren, Y. Xu, P. Li, H. Zhou, Boosting of electromagnetic wave absorption properties by multiple reinforcement mechanisms of metals in FeNi3/MoS2@NSAPC composites, Mater. Sci. Eng.: B 298 (2023) 116826.

[42] X. Huang, Y. Ma, H. Lai, Q. Jia, L. Zhu, J. Liu, B. Quan, Conductive substrates-based component tailoring via thermal conversion of metal organic framework for enhanced microwave absorption performances, J. Colloid Interface Sci. 608 (2022) 1323–1333.

[43] W. Liu, J. Pan, G. Ji, X. Liang, Y. Cheng, B. Quan, Y. Du, Switching the electromagnetic properties of multicomponent porous carbon materials derived from bimetallic metal–organic frameworks: effect of composition, Dalton Trans. 46 (2017) 3700–3709.

[44] K. Deng, H. Wu, Y. Li, J. Jiang, M. Wang, Z. Yang, R. Zhang, The resin-ceramic-based Fe3O4/graphite composites rapidly fabricated by selective laser sintering for integration of structural-bearing and broadband electromagnetic wave absorption, J. Alloy. Compd. 943 (2023) 169120.

[45] G. Wang, Z. Gao, S. Tang, C. Chen, F. Duan, S. Zhao, S. Lin, Y. Feng, L. Zhou, Y. Qin, Microwave absorption properties of carbon nanocoils coated with highly controlled magnetic materials by atomic layer deposition, ACS Nano 6 (2012) 11009–11017.

[46] Z. Liu, N. Zhao, C. Shi, F. He, E. Liu, C. He, Synthesis of three-dimensional carbon networks decorated with Fe3O4 nanoparticles as lightweight and broadband electromagnetic wave absorber, J. Alloy. Compd. 776 (2019) 691–701.

[47] Z. Liu, Y. Lv, J. Fang, X. Zuo, C. Zhang, X. Yue, A new method for an efficient porous carbon/Fe3O4 composite based electromagnetic wave absorber derived from a specially designed polyimide, Compos. Part B: Eng. 155 (2018) 148–155.

[48] Y. Deng, Y. Zheng, D. Zhang, C. Han, A. Cheng, J. Shen, G. Zeng, H. Zhang, A novel and facile-to-synthesize three-dimensional honeycomb-like nano-Fe3O4@C composite: Electromagnetic wave absorption with wide bandwidth, Carbon 169 (2020) 118–128.
[49] Y. Wang, M. Zhang, X. Deng, Z. Li, Z. Chen, J. Shi, X. Han, Y. Du, Reduced graphene oxide aerogel decorated with Mo2C nanoparticles toward multifunctional properties of hydrophobicity, thermal insulation and microwave absorption, Int. J. Miner., Metall. Mater. 30 (2023) 536–547.
[50] Y. Huang, W.-L. Song, C. Wang, Y. Xu, W. Wei, M. Chen, L. Tang, D. Fang, Multi-scale design of electromagnetic composite metamaterials for broadband microwave absorption, Compos. Sci. Technol. 162 (2018) 206–214.
[51] R. Qiang, S. Feng, Y. Chen, Q. Ma, B. Chen, Recent progress in biomass-derived carbonaceous composites for enhanced microwave absorption, J. Colloid Interface Sci. 606 (2022) 406–423.
[52] R. Qiang, Y. Du, D. Chen, W. Ma, Y. Wang, P. Xu, J. Ma, H. Zhao, X. Han, Electromagnetic functionalized Co/C composites by in situ pyrolysis of metal-organic frameworks (ZIF-67), J. Alloy. Compd. 681 (2016) 384–393.